Astronomical Techniques and Instruments, Vol. 2, September 2025, 288–298

Article Open Access

A target imaging simulation method for ground-based system based on signal-to-noise ratio

Chunxu Ren[1,2], Yun Li[1*], Yanzhao Li[1,2], Weihua Gao[1,2], Wenlong Niu[1], Xiaodong Peng[1,3]

[1]*National Space Science Center*, *Chinese Academy of Sciences*, *Beijing* 100190, *China*

[2]*University of Chinese Academy of Sciences*, *Beijing* 101408, *China*

[3]*National Key Laboratory of Deep Space Exploration*, *Hefei* 230000, *China*

*Correspondence: liyun02@nssc.ac.cn

Received: February 28, 2025; Accepted: May 8, 2025; Published Online: May 14, 2025; https://doi.org/10.61977/ati2025023; https://cstr.cn/32083.14.ati2025023

Citation: Ren, C. X., Li, Y., Li, Y. Z., et al. 2025. A target imaging simulation method for ground-based system based on signal-to-noise ratio. *Astronomical Techniques and Instruments*, **2**(5): 288−298. https://doi.org/10.61977/ati2025023.

Abstract: Space target imaging simulation technology is an important tool for space target detection and identification, with advantages that include high flexibility and low cost. However, existing space target imaging simulation technologies are mostly based on target magnitudes for simulations, making it difficult to meet image simulation requirements for different signal-to-noise ratio (SNR) needs. Therefore, design of a simulation method that generates target image sequences with various SNRs based on the optical detection system parameters will be important for faint space target detection research. Addressing the SNR calculation issue in optical observation systems, this paper proposes a ground-based detection image SNR calculation method using the optical system parameters. This method calculates the SNR of an observed image precisely using radiative transfer theory, the optical system parameters, and the observation environment parameters. An SNR-based target sequence image simulation method for ground-based detection scenarios is proposed. This method calculates the imaging SNR using the optical system parameters and establishes a model for conversion between the target's apparent magnitude and image grayscale values, thereby enabling generation of target sequence simulation images with corresponding SNRs for different system parameters. Experiments show that the SNR obtained using this calculation method has an average calculation error of <1 dB when compared with the theoretical SNR of the actual optical system. Additionally, the simulation images generated by the imaging simulation method show high consistency with real images, which meets the requirements of faint space target detection algorithm research and provides reliable data support for development of related technologies.

Keywords: Image SNR calculation; Imaging simulation; Ground-based optical detection system; Space target image sequence

1. INTRODUCTION

In recent years, with the rapid developments in aerospace technology, the number of spacecraft in orbit has shown a significant growth trend[1]. This trend has led to a continuous increase in the occupation of space orbit resources, gradual rises in the amount of space debris and the number of decommissioned satellites, and a significant increase in the risk of collisions between spacecraft, which poses a serious threat to the normal, safe operation of satellites in orbit. As a result, space situational awareness (SSA) has become a strategic focus for all countries to maintain safe operation of their spacecraft, ensure sustainable use of space resources, and enhance space security capabilities[2–4]. Dim space target detection technology, as an essential technology for SSA, can identify and monitor low-brightness and long-distance space targets effectively in complex space environments. This technology provides essential support to ensure both the safe operation of spacecraft in orbit and the sustainable use of space resources. This detection technology thus has significant engineering application value and has become an important direction for research and development in the aerospace field[5–8].

Dim space target detection methods can be divided into model-driven methods and data-driven methods. Model-driven methods are based on the use of mathematical theories to suppress the background and perform target enhancement. However, these methods require numerous assumptions and involve multiple parameters, making the calculations complex. In contrast, data-driven methods often use deep learning to learn the features of targets, thus enabling distinctions to be made between targets and the background. These methods have demonstrated strong robustness and accuracy, and have become the main development trend in this field[9]. However,

data-driven methods require large numbers of training images, and the acquisition of imaging data from actual observation systems is challenging[10]. These challenges have limited the development of space target detection algorithms.

Space target imaging simulation technology is one of the most effective approaches used to provide training images for target detection algorithms. This technique is used widely in both technical research and engineering applications for ground-based verification of equipment and algorithms[11].

As early as 2009, Zhang et al.[12] established a detailed simulation model by studying a combination of the transformation relationship from stellar magnitude to grayscale and the statistical patterns of star numbers. Their model can generate starry sky background images with relatively large magnitudes (magnitude > 10). Then, Han et al.[13] used Satellite Tool Kit (STK) software[14] (Analytical Graphics) to obtain the positional relationship between the target and the observation platform, and used OpenGL to render the simulation images to enhance the realism of the images that were generated. However, because of the complexity of the OpenGL rendering process, the algorithm ran slowly. To address this issue, Zhang et al.[15] used MATLAB rather than OpenGL to add various noise types and effects to the images to accelerate the algorithm's simulation speed.

Subsequently, to simulate the brightness characteristics of targets with different shapes in images, Yan et al.[16] proposed a target illumination model based on the effective optical reflective area, which addresses the conversion relationship between magnitude and grayscale, along with that between magnitude and pixel intensity. This conversion model uses a linear relationship that does not align fully with the nonlinear characteristics of actual complex optical imaging scenarios, which limits its accuracy and its wider applicability. To solve this problem, Xia et al.[11] used an exponential conversion relationship to perform the transformation between magnitude and grayscale, which is more closely aligned with actual complex optical imaging scenarios, and also conducted a simulation analysis of the image characteristics under the different system monitoring mode conditions. This method alleviates the limitations of the linear conversion model effectively, but it does not account for the effects of the system parameters and environmental factors on the target's brightness during the actual imaging process.

In addition, to make the simulations more realistic, Ouyang et al.[17] proposed a method to simulate optical images of space debris for use with a small field-of-view (FOV), high-detection-sensitivity space imaging system that considered the interference from stripes and the saturated star background. Wang et al.[18] also considered the effects of stray light, including ground-based light and moonlight, on the optical detection system and established a stray light imaging simulation model. Based on this model, Liu et al.[19] modeled the imaging process under the platform jitter condition by applying a jitter effect to the simulated images to enhance their realism. Additionally, to evaluate the performance of wide-field sensors, Xu et al.[20] implemented space imaging simulations based on the characteristics of a panoramic scanning sensor to generate a sequence of images that covered a 360° × 10° FOV. Although these methods analyzed the factors that affected optical target imaging under various observation conditions, they did not establish the corresponding relationship between the observation conditions and the SNR of the image, thus making it difficult to provide target data with differing SNRs for target detection algorithms.

At present, space target imaging simulations use a relatively well-established technical framework, and the simulation results obtained are quite close to real-world scenarios. However, these existing simulation methods do not take the impact of the observation system parameters and environmental factors on the target brightness into account when calculating the brightness, and they also do not define the relationship between the SNR and the target image grayscale values clearly. As a result, these methods are still unable to generate images with a specified SNR based on the system parameters of the observation platform, particularly for target imaging under low SNR conditions. This makes it difficult for the existing simulation methods to meet the demand for training data with different SNRs as required for weak space target detection technology. Therefore, the work in this paper uses a ground-based optical detection system as an example, with dynamic imaging of small space targets as the simulation target, and it also conducts space target imaging simulation research based on the SNR for the starry sky background. The main contributions are described as follows:

(1) A ground-based detection image SNR calculation method based on the optical system parameters is proposed. Based on the apparent target magnitude, system parameters such as the operational spectral range, the quantum efficiency, the effective aperture, the optical transmittance, the exposure time, and the noise parameters of the ground-based optical detection system, and the observation environment parameters, the method can calculate the image SNR under various observation conditions.

(2) A target sequence image simulation method based on the SNR for ground-based detection scenarios is also proposed. The method calculates the image SNR under the current observation conditions based on the observation system parameters and establishes the conversion relationship between the target magnitude and grayscale based on the SNR; then, it obtains the target motion model from the target orbital data, thereby realizing simulation of the target sequence images.

2. METHODS

2.1. Apparent Magnitude Calculation

The magnitude is an important indicator for measure-

ment of the brightness of celestial objects and typically includes two types: the absolute magnitude and the apparent magnitude. Modern astronomy uses a logarithmic scale to describe brightness differences. Specifically, a reduction of five magnitudes corresponds to a 100-fold increase in the brightness of the celestial object[21].

The absolute magnitude is a standardized measure of brightness that reflects the intrinsic luminosity of an astronomical object and is unaffected by its distance from the observer. For stellar objects, the absolute magnitude refers to the apparent magnitude that an object would have if placed at a distance of 10 parsecs. The absolute magnitude for non-stellar objects such as planets, comets, and asteroids is defined as the apparent magnitude that the object would exhibit when it is located at a distance of one astronomical unit (AU) from both the Sun and Earth with a phase angle of 0°. Additionally, the absolute magnitude of non-stellar objects can also be calculated using the following formula[22]:

$$H = 15.618 - 5\lg D - 2.5\lg P_{\mathrm{v}}\,, \tag{1}$$

where D is the object diameter and P_{v} is surface albedo of the object.

The apparent magnitude refers to the brightness of an astronomical object as observed from the Earth. The apparent magnitude is dependent on the object's intrinsic luminosity and the distance between the object and the Earth. Additionally, the apparent magnitude is strongly affected by the absorption properties of dust, gas, and other media located between the object and the Earth. Variations in observational angle and atmospheric conditions can further modulate its value. For stellar objects, there is a specific conversion relationship between the apparent magnitude and the absolute magnitude, which can be expressed as

$$M = m + 5\lg\left(\frac{d_0}{d}\right), \tag{2}$$

where d_0 is 10 parsecs and d is the distance from the observer to the object.

For celestial bodies that do not emit their own light, e.g., planets and asteroids, their apparent magnitude is related to the solar phase angle. The equation used to calculate this magnitude[23]is as follows:

$$V = H + 2.5\lg\left\{\left(\frac{|\boldsymbol{r}_{\mathrm{sun}}|}{1.5\times10^{8}}\times\frac{|\boldsymbol{r}_{\mathrm{obs}}|}{1.5\times10^{8}}\right)^{2} - \left[(1-G)\varphi_1 + G\varphi_2\right]\right\}, \tag{3}$$

where H is the absolute magnitude of the object; $\boldsymbol{r}_{\mathrm{sun}}$ and $\boldsymbol{r}_{\mathrm{obs}}$ are vectors from the Sun to the asteroid and from the observer to the asteroid, respectively; G is the surface albedo of the asteroid; and φ_1 and φ_2 are phase functions, which are given by

$$\varphi_1 = \mathrm{e}^{-3.33\tan k^{0.63}}\,, \tag{4}$$

$$\varphi_2 = \mathrm{e}^{-1.87\tan(k/2)^{1.22}}\,, \tag{5}$$

where k is the angle between $\boldsymbol{r}_{\mathrm{sun}}$ and $\boldsymbol{r}_{\mathrm{obs}}$.

For nonluminous targets, e.g., space debris[24], the calculation of their apparent magnitude is related to the phase function, and the method is given as follows:

$$V = -26.58 - 2.5\lg\left[A\sigma F(\varphi)\right] + 5\lg R\,, \tag{6}$$

where A is the cross-sectional area of the target; σ is the diffuse reflection coefficient of the target, $F(\varphi)$ is the phase function of the target, φ is the solar phase angle of the target, and R is the distance between the observer and the target.

2.2. SNR Calculation Method for Ground-based Systems

Based on the methods described above for the calculation of the apparent magnitude of a target, we can obtain the apparent magnitude under different observation scenarios. To establish the conversion relationship between the target magnitude and the SNR, this paper proposes an SNR calculation method that is suitable for ground-based systems. This method integrates the target's radiative transfer characteristics, the observation system parameters, and the environmental factors, while also comprehensively considering the imaging process of the optical system, the detector's noise characteristics, and the sky background interference to calculate and obtain the target's SNR within the image.

First, the celestial objects that are observable by ground-based systems mainly include asteroids, planets, and various small space objects. These objects emit light by reflecting sunlight and can therefore be reasonably approximated as blackbodies during modeling. The spectral radiance that corresponds to each wavelength can be calculated using the Planck formula as follows:

$$M(\lambda, T) = \frac{2hc^2}{\lambda^5\left(\mathrm{e}^{hc/\lambda k_{\mathrm{B}}T} - 1\right)}\,, \tag{7}$$

where h is Planck's constant, where $h = 6.626 \times 10^{-34}$ J s; c is the speed of light; T is the surface temperature of the Sun; and k_{B} is the Boltzmann constant, where $k_{\mathrm{B}} = 1.38 \times 10^{-23}$ J K^{-1}.

Then, according to the Stefan–Boltzmann law, the spectral photon flux density of a target with an apparent magnitude of zero can be obtained, as shown in the following equation:

$$I(\lambda, T) = \frac{f_{\odot}2.512^{-(BC-m_{\mathrm{b}\odot})}}{hc/\lambda}\frac{M(\lambda, T)}{\sigma T^4}, \tag{8}$$

where BC is the thermal magnitude correction parameter; $f_{\odot}$ is the solar constant, where $f_{\odot} = 1\,367.51$ W m^{-2}; σ is the Stefan–Boltzmann constant, where $\sigma = 5.67 \times 10^{-8}$ W m^{-2} K^{-4}; and $m_{\mathrm{b}\odot}$ is the apparent thermal magnitude of the Sun.

Then, the number of electrons N_T that the imaging sensor can generate during the imaging time at the different wavelengths is given by

$$N_T = \int_{\lambda_1}^{\lambda_2} I(\lambda, T)\mathrm{d}\lambda \cdot QE \cdot \frac{\pi}{4} d^2 \cdot \gamma \cdot t_0 \cdot 2.512^{-mV}, \quad (9)$$

where $\lambda_1 - \lambda_2$ represents the operational spectral range of the detector, which is typically taken to be the visible light spectrum (400–800 nm); QE is the quantum efficiency of the detector; d is the effective aperture of the telescope; γ is the optical transmittance; t_0 is the exposure time; and mV is the apparent magnitude of the target.

During the imaging process, the main noise sources include the noise generated by the sky background and the internal noise of the detector. The sky background brightness is typically represented by the parameter SQM, which has units of mag arcsec^{-2}. The equation for calculation of the sky background noise is given as follows:

$$N_{bg} = \int_{\lambda_1}^{\lambda_2} I(\lambda,T)\mathrm{d}\lambda \cdot QE \cdot \frac{\pi}{4} d^2 \cdot \gamma \cdot t_0 \cdot 2.512^{-SQM} \cdot p_{fov}, \quad (10)$$

where p_{fov} is the FOV of a single pixel in the detector. If p_{fov} cannot be obtained directly, it can be calculated using the following equation:

$$p_{fov} = \frac{W/f \times 206\,265}{pixel\_x} \times \frac{H/f \times 206\,265}{pixel\_y}, \quad (11)$$

where W and H are the width and the height of the detector's photosensitive element surface, respectively; f is the focal length of the telescope; and $pixel\_x$ and $pixel\_y$ are the numbers of pixels (resolution) of the detector's image sensor in the x and y directions, respectively.

The internal noise of the detector mainly comprises the readout noise (N_r) and the dark current noise (N_{dim}), and their values can be found in the detector's manual. The SNR of the detector can then be expressed using the following equation:

$$R_{SN} = \frac{N_T/p}{\sqrt{N_{bg} + N_r^2 + N_{dim} \times t_0}}, \quad (12)$$

where p represents the pixel size occupied by the target in the image.

2.3. Target Sequence Image Simulation Method in Ground-based Detection Scenes

Based on the SNR calculation method above, a target sequence image simulation method for ground-based detection scenes is proposed, as shown in the overall process flowchart given in Fig. 1.

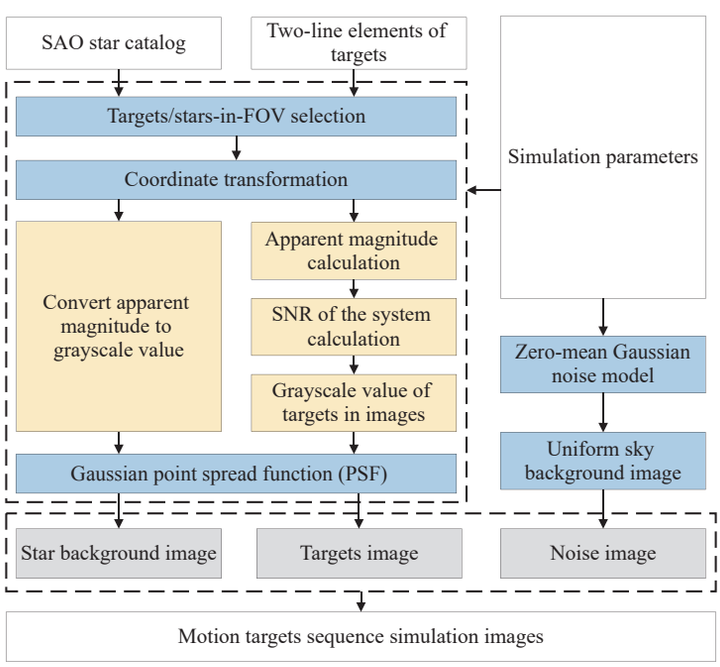

Fig. 1. Overall flowchart for the target sequence image simulation method in ground-based detection scenarios.

First, the positions and magnitudes of the stars in the J2000.0 geocentric inertial coordinate system are obtained based on the data from the Smithsonian Astrophysical Observatory (SAO) Star Catalog. Additionally, the target's position in the J2000.0 geocentric inertial coordinate system is obtained using the simplified general perturbations SGP4 orbital model based on the target's two-line element (TLE) orbital data.

Next, based on the simulation parameters, the targets and stars that lie within the FOV are selected. The observation field is generally regarded as a circular FOV with its center at the pointing direction of the observation platform's optical axis, and a radius that is half of the diagonal of the observation platform's FOV. Targets and stars within this circular FOV can then be observed by the platform. The constraint condition for the object within the

observation FOV is expressed as follows:

$$\begin{cases} \alpha \in (\alpha_0 - R/\cos\delta_0,\ \alpha_0 + R/\cos\delta_0) \\ \delta \in (\delta_0 - R,\ \delta_0 + R) \end{cases}, \tag{13}$$

where R is the radius of the circular observation field, and (α_0, δ_0) is the pointing direction of the starboard sensor's optical axis.

Then, the positions of the stars and the targets within the FOV are transformed into the image plane coordinate system. The coordinate transformation process includes a rotation transformation from the J2000.0 geocentric inertial coordinate system into the observation platform camera's coordinate system, and a perspective projection transformation from the observation platform camera coordinate system into the image plane coordinate system. The formula used to perform this transformation is shown as follows:

$$\boldsymbol{M}_{\mathrm{r}} = \begin{bmatrix} \sin\alpha_0\cos\phi_0 - \cos\alpha_0\sin\beta_0\sin\phi_0 & -\cos\alpha_0\cos\phi_0 - \sin\alpha_0\sin\beta_0\sin\phi_0 & \cos\beta_0\sin\phi_0 \\ -\sin\alpha_0\sin\phi_0 - \cos\alpha_0\sin\beta_0\cos\phi_0 & \cos\alpha_0\sin\phi_0 - \sin\alpha_0\sin\beta_0\cos\phi_0 & \cos\beta_0\cos\phi_0 \\ -\cos\alpha_0\cos\beta_0 & -\sin\alpha_0\cos\beta_0 & -\sin\beta_0 \end{bmatrix}, \tag{14}$$

$$\boldsymbol{M}_{\mathrm{p}} = \begin{bmatrix} f/z & 0 & pixel/2 \\ 0 & f/z & pixel/2 \\ 0 & 0 & 0 \end{bmatrix}, \tag{15}$$

where $\boldsymbol{M}_{\mathrm{r}}$ and $\boldsymbol{M}_{\mathrm{p}}$ are the rotation transformation matrix and the perspective projection transformation matrix, respectively; $(\alpha_0, \delta_0, \phi_0)$ are the right ascension, the declination, and the camera rotation angle of the observation platform in the J2000.0 geocentric inertial system, respectively; and z is the projection position of the target or star on the z-axis of the observation platform camera's coordinate system.

Then, the position of the target or star with coordinates $(x_{\mathrm{t}}, y_{\mathrm{t}}, z_{\mathrm{t}})$ in the J2000.0 geocentric inertial system is given in the image plane coordinate system as follows:

$$\begin{bmatrix} X \\ Y \\ 0 \end{bmatrix} = \boldsymbol{M}_{\mathrm{p}} \cdot \boldsymbol{M}_{\mathrm{r}} \begin{bmatrix} x_{\mathrm{t}} \\ y_{\mathrm{t}} \\ z_{\mathrm{t}} \end{bmatrix}. \tag{16}$$

Additionally, it is necessary to convert the star's apparent magnitude into the corresponding grayscale value in the image. For stars, the brightness differs between two stars with adjacent unit magnitudes by approximately 2.512 times. Therefore, the grayscale value of a star with apparent magnitude m_i can be calculated based on the observation system's magnitude sensitivity m, as follows:

$$g_i = \frac{g_{\max}}{2.512^{m_i - m}}, \tag{17}$$

where $g_{\max}$ is the grayscale value that corresponds to the brightest magnitude (255 in an 8-bit grayscale image).

At the same time, the conversion relationship between the target's apparent magnitude and its grayscale value can be obtained based on the SNR, the background noise mean, and the background noise variance of the image. The target's apparent magnitude is calculated using the corresponding formula based on the target type mentioned above. The SNR of the image is the ratio of the grayscale mean in the target region to the standard deviation in the noise region. Because the system's SNR is equal to the SNR of the simulated image, after the SNR of the system's image is calculated using the simulation parameters, the grayscale mean of the target in the image can then be deduced as follows:

$$\bar{g}_{\mathrm{t}} = R_{\mathrm{SN}}\sigma_{\mathrm{n}} + \bar{g}_{\mathrm{n}}, \tag{18}$$

where R_{SN} is the SNR that corresponds to the target's apparent magnitude; $\bar{g}_{\mathrm{n}}$ is the mean grayscale value of the uniform background in the simulation image; and σ_{n} represents the standard deviation of the Gaussian noise in the simulation image.

In ground-based long-distance detection scenarios, the target and the stars are located far away from the telescope, and their signals can be regarded as point light sources. After passing through the optical system, these signals present an approximately Gaussian distribution within a local region of the image. Therefore, the Gaussian PSF model can be used to approximate the grayscale distribution of the target and the stars.

The equation for the Gaussian PSF is as follows:

$$g(x_i, y_i) = A\exp\left[-\frac{(x_i - x_0)^2 + (y_i - y_0)^2}{2\sigma^2}\right], \tag{19}$$

where A is the grayscale value at the center of the target or star; (x_0, y_0) and (x_i, y_i) are the pixel coordinates of the star spot center and the pixel coordinates of the ith point of the target or star, respectively; and σ is the standard deviation of the PSF, which can be calculated using the following:

$$\sigma = \frac{w}{2\sqrt{-\lg(1 - p_{\mathrm{r}})}}, \tag{20}$$

where w is the width of the target or star, and p_{r} is the percentage of the starlight energy contained within the width range.

We obtain the grayscale value at the target's center via reverse engineering based on the target's grayscale mean value and the Gaussian PSF. The equation required is as follows:

$$A = \frac{\bar{g}_{\mathrm{t}} p}{\sum_{i=0}^{p} \exp\left[-\frac{(x_i - x_0)^2 + (y_i - y_0)^2}{2\sigma^2}\right]}. \tag{21}$$

Finally, the noise image obtained by adding the zero-mean Gaussian noise and the uniform background is synthesized with the target image and the star background image to obtain the final target sequence simulation image.

3. EXPERIMENT

In this work, experiments were conducted to verify the accuracy of the proposed SNR calculation method and the accuracy and the simulation effectiveness of the proposed target sequence image simulation method.

For the proposed SNR calculation method, images of specified celestial objects must first be captured using a designated instrument with different exposure times. The actual SNR for the captured image sequences will then be computed. Next, the theoretical SNR can be calculated using the proposed method with the observation parameters and the celestial object's apparent magnitude. The accuracy of the proposed method can then be validated by comparing the theoretical and actual SNR values to determine the error between them.

For the proposed target sequence image simulation method, observations must first be conducted on a designated sky region using the specified observation parameters, and the corresponding background star simulation images will then be generated. These simulated images will then be compared with the actual telescope images of the corresponding sky region to check whether the positions of the stars match, thus confirming the accuracy of the proposed simulation method. Subsequently, multiple sets of target sequence simulation data will be generated by adjusting the various exposure times, and the SNR variations between the different sequences will then be observed to evaluate the effectiveness of the simulation method.

3.1. Accuracy Verification Experiment for the Proposed SNR Calculation Method

At the Huairou Campus of the National Space Science Center of the Chinese Academy of Sciences, we conducted observational experiments using a Celestron C11HD Schmidt-Cassegrain telescope paired with a ZWO ASI174MM planetary camera. The weather on the day was clear with no moon, but the light pollution was relatively severe, with an SQM index of 19.75 mag arcsec^{-2}. We observed Saturn and its moons, along with the star SAO 93495. The telescope parameters are given in Table 1 and the planetary camera parameters are listed in Table 2.

Six data sets were collected from the experiments. These sets included three sets of observational data for Saturn and its moons, which were captured with exposure times of 0.3 s, 0.1 s, and 0.02 s; and three sets of observational data of Uranus and SAO 93495 that were acquired using exposure times of 0.5 s, 0.2 s, and 0.1 s. The images of Saturn and its moons are shown in Fig. 2, and the images of Uranus and SAO 93495 are shown in Fig. 3.

Table 1. Parameters of the telescope and their settings

Parameter	Value
Optical system	HD Schmidt-Cassegrain
Aperture/mm	279.4
Focal length/mm	2800
Focal ratio	10.02
Finderscope	9 × 50
Optical coating	Starbright XLT Coating
Optical efficiency/(%)	≈ 89

Table 2. Parameters of the planetary camera and their settings

Parameter	Value
Sensor	IMX174LLJ-C
Sensor size/(")	1/1.2
Resolution	2.3 Megapixels 1936 × 1216
Pixel size/μm	5.86
Target size	11.345 mm × 7.125 mm
Exposure time	32 μs–300 s
Readout noise	3.5 e^- @ 30 dB gain
Peak QE/(%)	78
Full well charge	32 000 e^-
Analog-to-Digital Converter/bit	12 /10

In the Saturn observation images, both Titan and Hyperion are located far away from Saturn and are less strongly affected by the diffused light from Saturn. Therefore, the SNRs of these two moons in the image are calculated primarily. In the Uranus observation data, Uranus has a higher magnitude, and the charge received by the target pixels in the charge-coupled device (CCD) in the detector reaches the saturation charge level. As a result, reducing the exposure time does not affect the SNR significantly. Therefore, the SAO 93495 star within the FOV is selected to calculate the SNR in this case.

By inputting the target's apparent magnitude, the exposure time, the pixel size, the telescope parameters, and the detector parameters into the proposed SNR calculation method, both the S/N SNR and the dB SNR calculation results are obtained. The target's name, the target's apparent magnitude, the target's pixel size, the exposure time, the actual SNR, and the calculated theoretical SNR are listed in Table 3.

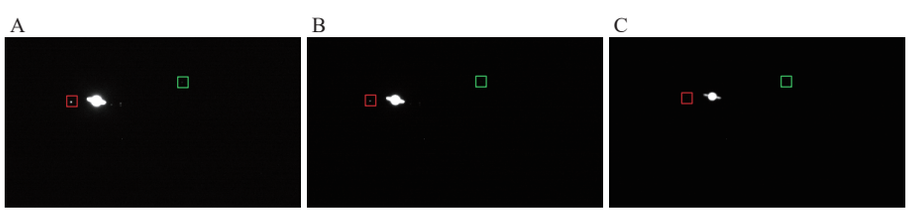

Fig. 2. Sample images of Saturn and its moons acquired during the observation with an exposure time of (A) 0.3 s; (B) 0.1 s; (C) 0.02 s. In all images, Titan is located in the red box and Hyperion is located in the green box.

Fig. 3. Sample images of Uranus and SAO 93495 acquired during the observation with an exposure time of (A) 0.5 s; (B) 0.2 s; (C) 0.1 s. In all images, SAO 93495 is located in the red box, and Uranus is located in the green box.

Table 3. Actual SNR and theoretical SNR values calculated using the proposed method for the celestial objects in the collected observational images. The data in bold in the table represent the maximum values for the current parameters

Target name	Apparent magnitude /mV	Exposure time /s	Target pixel count	Actual SNR		Calculated SNR		Error between two SNRs	
				S/N	dB	S/N	dB	S/N	dB
Titan	8.42	0.3	13 × 13	7.002	8.452	7.643	8.830	0.641	0.378
		0.1	13 × 13	5.868	7.685	5.046	7.029	**0.822**	0.656
		0.02	13 × 13	1.097	0.421	0.897	−0.472	0.200	0.893
Hyperion	11.21	0.3	7 × 7	1.800	2.553	1.728	2.375	0.072	0.178
		0.1	7 × 7	1.000	0.000	0.893	−0.491	0.107	0.491
		0.02	7 × 7	0.143	−8.446	0.200	−6.984	0.057	**1.462**
SAO 93495	9.2	0.5	11 × 11	5.076	7.055	5.122	7.094	0.046	0.039
		0.2	8 × 8	3.933	5.947	3.414	5.332	0.519	0.615
		0.1	8 × 8	3.592	5.553	3.061	4.859	0.531	0.694

Table 3 shows that the results obtained using the proposed SNR calculation method have maximum errors of 0.822 (S/N) and 1.462 (dB) when compared with the actual observed SNR, with average errors of 0.331 (S/N) and 0.601 (dB). For the S/N SNR, the error between the results obtained from the proposed method and the actual observed SNR does not exceed 1. However, for the dB SNR, because the dB SNR and the S/N SNR have a logarithmic relationship, the dB SNR compresses the variation of the S/N SNR when the S/N SNR > 1, and it amplifies the variation of the S/N SNR when the S/N SNR < 1. Therefore, when the S/N SNR < 1, even a small error can lead to a significant difference in the dB SNR results. As a result, the maximum error in the dB SNR is relatively large, but for the positive dB SNR values, the maximum error is 0.694. From the average error between the actual SNR and the calculated theoretical SNR, it can be concluded that the average calculation error of the proposed SNR calculation method is <1 dB. Although there are some errors, the results remain within the same order of magnitude as the actual SNR, thus indicating that the method has significant reference value. The proposed method can reflect the SNR of a target in an image realistically under specific observational conditions.

3.2. Experiment of the Proposed Target Sequence Image Simulation Method

3.2.1. *Accuracy verification experiment for the proposed simulation method*

We compared the background star simulation images of a designated sky region that were generated using the simulation algorithm under specified observation conditions with images captured by the Guan Sheng Optical (GSO) 8-inch RC reflecting telescope. By comparing the relative positions of multiple stars in the corresponding images, we verified the accuracy of the proposed simulation algorithm.

We selected the typical Pleiades cluster as the observation target. The observation parameters, which are given in Table 4, include the observation time, the observation location, the FOV angle, the telescope axis orientation, the image resolution, and the camera focal length. The background star image generated using the simulation algorithm is shown in Fig. 4A, and the corresponding sky region image captured by the GSO 8-inch RC reflecting telescope is shown in Fig. 4B.

Table 4. Observation parameters used for the simulation-generated data of the Pleiades cluster

Parameter	Value
Observation time (UTC)	2025−01−25 06:30:00
Observation location	Longitude 116° Latitude 39° Altitude 49 m
Observation axis direction	Right ascension 56.62° Declination 24.21°
Observation FOV	1.12° × 1.12°
Image resolution	500 × 500
Focal length	150 mm

In Fig. 4, we compared the positions of 17 stars in the Pleiades cluster image generated by the simulation algorithm with the corresponding positions of these stars in the image of the Pleiades cluster captured by the GSO 8-inch RC reflecting telescope. The figure shows that the simulated results align well with the actual distribution of the

background stars in the captured image. However, some stars observed in the actual captured image were not found as corresponding star points in the simulation results. These differences may be caused by two factors: on the one hand, the SAO Star Catalog does not contain a complete list of star entries, and on the other hand, the observational parameters that we selected caused stars with relatively low apparent magnitudes to have smaller grayscale values in the image, thus making them undetectable.

Additionally, the simulation results also show that the star spots for stars with higher magnitudes are larger. This occurs because stars with higher magnitudes emit stronger light, which leads to the higher brightness in the image. As a result, when simulating using the PSF, the star spot formed has a larger extent.

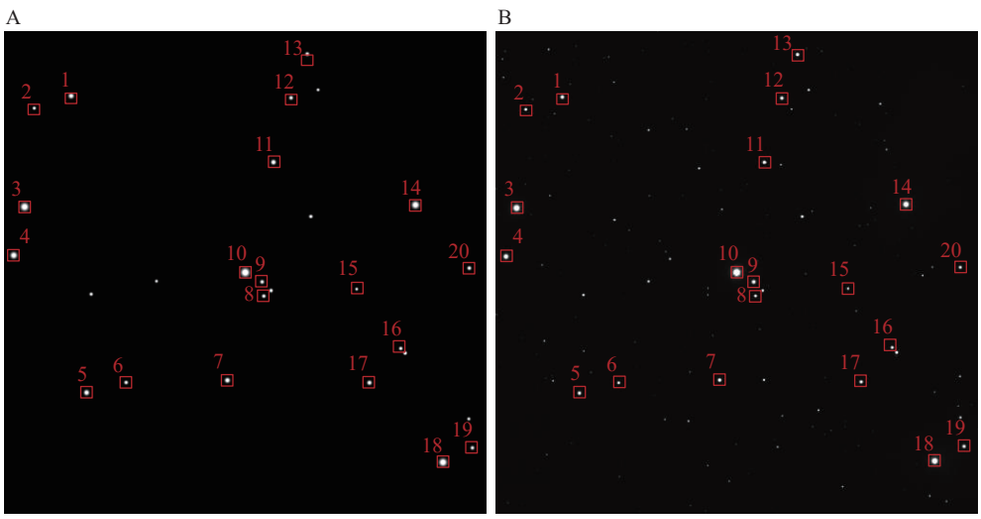

Fig. 4. Results of comparison of the simulation-generated Pleiades cluster image with the Pleiades cluster image captured by the Guan Sheng Optical (GSO) 8-inch RC reflecting telescope. (A) Simulation-generated Pleiades cluster image. (B) Pleiades cluster image captured by the GSO 8-inch RC reflecting telescope. The stars enclosed in the red boxes are used for the comparison, and stars with the same number represent the comparison results for the same star.

3.2.2. *Simulation Experiment of Target Sequence Images Acquired under Different Observation Parameters*

Based on the proposed target sequence image simulation algorithm for ground-based scenarios, we simulated multiple observation data sets for the DSCS 2-2 satellite (OPS 9432) with different exposure times.

The physical characteristics and the orbital information of the satellite are presented in Table 5. The DSCS 2-2 satellite (OPS 9432) has an average diameter of 1.42 m and a surface albedo of 0.2. By assuming that the satellite's cross-section is circular, the calculated apparent magnitude under the given observational conditions is 13.08.

The simulation parameters of the algorithm were set as shown in Table 6. We simulated the sequence of motion images of the DSCS 2-2 satellite (OPS 9432) observed in Beijing for 100 s starting from 06:30:00 UTC on January 25, 2025, with exposure times of 0.1 s, 0.2 s, 0.3 s, and 0.5 s. The sky background brightness for that day was set at 19.75 mag arcsec^{-2}, and the telescope's optical axis was pointed at a right ascension of 132.47° and a declination of 3.75°. In addition, we set the target pixel size to be 3 × 3.

The SNR calculation results for the target observation data recorded over different exposure times as generated using the simulation algorithm are given in Table 7. The exposure times for Seq. 1, Seq. 2, Seq. 3, and Seq. 4 are 0.1 s, 0.2 s, 0.3 s, and 0.4 s, respectively. The average SNR for Seq. 1 is −1.12 dB and represents the minimum, while the average SNR for Seq. 4 is 4.83 dB and represents the maximum. It can thus be observed that the SNR of the target observation data increases with increasing exposure time, which aligns with the actual observation conditions.

The simulation results for the target sequence images

Table 5. Physical characteristics and orbital information of the DSCS 2-2 satellite (OPS 9432)

Category	Parameter	Value
Physical characteristics	Apparent magnitude/Mv	13.08
	Surface albedo	0.2
	Mean diameter/km	0.001 42
	Mass/kg	520.0
Orbital information	Eccentricity	0.000 293 1
	Semi-major axis/km	42 129
	Periapsis distance/km	35 742.8
	Orbital inclination/(°)	3.054 3
	Longitude of ascending node/(°)	270.023 2
	Argument of periapsis/(°)	24.822 8
	Mean argument of periapsis/(°)	206.392 8
	Orbital period/min	1 434.3
	Mean speed/(°/d)	358.571 6
	Aphelion distance/km	35 773.8

Table 6. Simulation parameters set for the ground-based target sequence image simulation algorithm

Parameter	Value
Observation time (UTC)	2025−01−25 6:30:00
Observation location	(116°, 39°, 49 m)
Observation axis direction	(132.47°, 3.75°)
Simulation duration/s	100
CCD sensor size/mm^2	2.93 × 2.93
CCD pixel size/μm	5.86
Focal length/mm	150
Sky background brightness/mag arcsec^{-2}	19.75
Quantum efficiency	0.7
Optical system transmittance	0.8
Readout noise/e$^-$ pixel^{-1} s^{-1}	3.5
Dark current noise/e$^-$ pixel^{-1} s^{-1}	0.01
CCD gain/e$^-$ ADU^{-1}	1.2
Camera aperture diameter/m	0.5
Exposure time/s	0.1, 0.2, 0.3, 0.5

generated using the proposed algorithm over different exposure times are shown in Fig. 5. Based on the exposure times, we generated four sets of target sequence simulation images, with each set comprising four images captured at 0 s, 10 s, 20 s, and 30 s intervals from the start of the observation. The DSCS 2-2 satellite is highlighted within the red box in each image. As the exposure time increases, both the target brightness and the background brightness in the image also increase. Additionally, the position of the DSCS 2-2 satellite in the image also shifts with the changes in the observation time.

Table 7. Exposure times and average SNR values for the four sets of sequence images generated using the target sequence image simulation algorithm in the ground-based detection scenario

Sequence number	Exposure time/s	Average SNR/dB
Seq. 1	0.1	−1.12
Seq. 2	0.2	1.58
Seq. 3	0.3	3.07
Seq. 4	0.5	4.83

Therefore, the proposed target sequence image simulation algorithm for ground-based detection scenarios is able to generate target observation data with varying SNRs under different observational conditions based on the input observation parameters. The algorithm takes several factors into account, including the exposure time, the telescope aperture, and other relevant parameters, to simulate image data that reflect the actual observations. In addition, the algorithm is able to simulate the target's motion over time. By incorporating the target's orbital parameters and trajectory into the simulation, it can model the dynamic changes in the target's position and orientation within the image field accurately. This enables the algorithm to generate time-series image sequences that reflect the actual motion of the target in space.

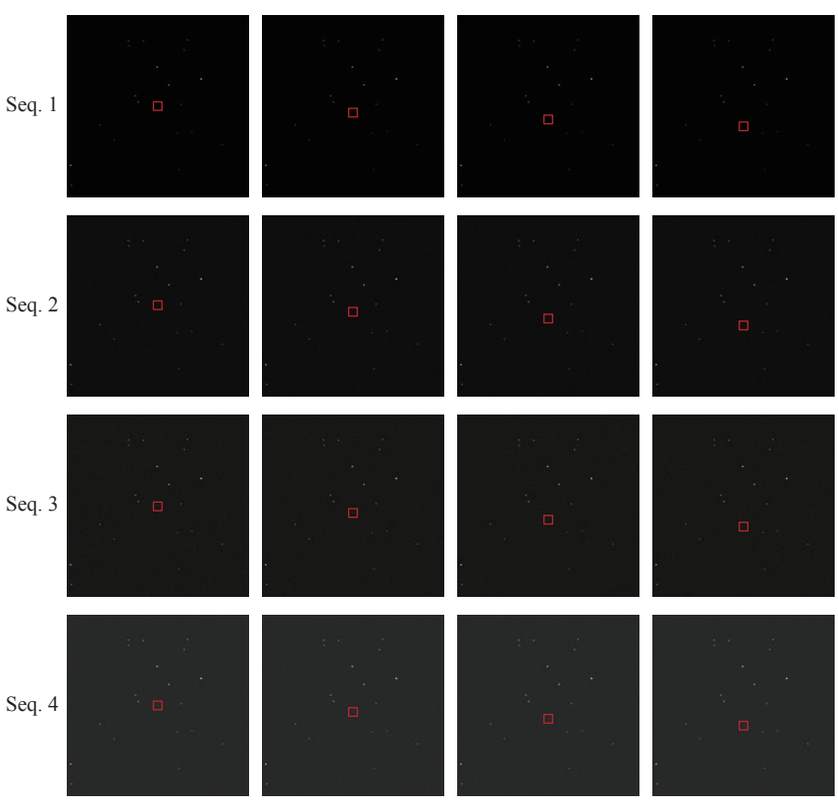

Fig. 5. Four simulation result sets from the target sequence image simulation algorithm for ground-based detection scenarios under specified observational conditions, where each sequence consists of four target simulation images captured at 0 s, 10 s, 20 s, and 30 s intervals from the start of observation. Seq. 1, Seq. 2, Seq. 3, and Seq. 4 are the target sequence simulation images acquired under exposure times of 0.1 s, 0.2 s, 0.3 s, and 0.5 s, respectively.

4. DISCUSSION

The SNR results obtained from the proposed ground-based system's SNR calculation method still show a small error when compared with the actual observed data. On the one hand, this may be caused by the influence of atmospherics on the actual observed images, where the target is not of a regular shape, and this would lead to some errors in the SNR values calculated from the actual observation data. On the other hand, the proposed SNR calculation method assumes a constant quantum efficiency for the observation system, whereas in reality, this efficiency varies with the spectral wavelength. In future work, we will consider using a variable quantum efficiency and attempt to account for the atmospheric effects on the observed target to improve the accuracy of the SNR calculation method.

The proposed target sequence image simulation method for ground-based detection scenarios is able to simulate target observation data with varying SNRs under different observational conditions. However, its observational scenarios have been limited to ground-based detection to date. In future work, we will explore the development of an SNR-based target sequence image simulation method for space-based detection scenarios and will design a simulation system to support practical application requirements.

5. CONCLUSIONS

We have proposed an SNR calculation method for ground-based systems and validated the method's accuracy using actual captured images. The calculated results showed an error of less than 1 dB when compared with the measured data. Based on this SNR calculation method, we have also introduced a target sequence image simulation method for ground-based scenarios. This method can simulate target observation data under various observational conditions, and the simulated star maps aligned well with the actual star maps. The method is able to simulate target trajectories and other dynamic aspects accurately. This simulation method provides a solid data foundation for research into weak space target detection algorithms and holds significant practical application value.

ACKNOWLEDGEMENTS

This work was supported by Open Fund of National Key Laboratory of Deep Space Exploration (NKDSEL2024014) and by Civil Aerospace Pre-research Project of State Administration of Science, Technology and Industry for National Defence, PRC(D040103).

AI DISCLOSURE STATEMENT

AI-assisted technology is not used in the preparation of this work.

AUTHOR CONTRIBUTIONS

Chunxu Ren conceived the ideas, designed and implemented the study, and wrote the paper. Yun Li， Wenlong Niu and Xiaodong Peng provided supervision and guidance throughout the study, and were responsible for project administration and funding acquisition, and contributed to manuscript review and editing. Yanzhao Li assisted with experimental procedures and data collection, and participated in manuscript revision and proofreading. Weihua Gao conducted literature review and provided relevant supporting materials. All authors read and approved the final manuscript.

DECLARATION OF INTERESTS

The authors declare no competing interests.

REFERENCES

[1] Bi, J. K., Xiao, W. P., He, H. D. 2024. Global space launch statistics in 2023. *Space International*, (2): 12−16. (in Chinese)

[2] Gill, E., Akos, D. M. 2024. Snapshot GNSS receivers for low-effort, high-gain space situational awareness. *Advances in Space Research*, **73**(1): 42−52.

[3] Xue, C. B., Cai, H., Gehly, S., et al. 2024. Review of sensor tasking methods in Space Situational Awareness. *Progress in Aerospace Sciences*, **147**: 101017.

[4] Barbosa, D., Coelho, B., Bergano, M., et al. 2024. PASO--Astronomy and Space Situational Awareness in a Dark Sky Destination. *arXiv: 2404.04090.*

[5] Karpukhin, V., Oğuz, B., Min, S., et al. 2020. Dense Passage Retrieval for Open-Domain Question Answering. *arXiv: 2004.04906*.

[6] Zhao, M. J., Li, W., Li, L., et al. 2022. Single-frame infrared small-target detection: A survey. *IEEE Geoscience and Remote Sensing Magazine*, **10**(2): 87−119.

[7] Yang, B., Zhang, X. Y., Zhang, J., et al. 2024. EFLNet: Enhancing feature learning network for infrared small target detection. *IEEE Transactions on Geoscience and Remote Sensing*, **62**: 5906511.

[8] Zhu, R., Fu, Q., Liu, N., et al. 2024. Improved target detection method for space-based optoelectronic systems. *Scientific Reports*, **14**: 1832.

[9] Zhang, F., Lin, S. L., Xiao, X. Y., et al. 2024. Global attention network with multiscale feature fusion for infrared small target detection. *Optics & Laser Technology*, **168**: 110012.

[10] Suthakar, V., Sanvido, A. A., Qashoa, R., et al. 2023. Comparative analysis of Resident Space Object (RSO) detection methods. *Sensors*, **23**(24): 9668.

[11] Xia, S. F., Chen, J. Y., Lei, X. X., et al. 2020. Space debris space-based monitoring image simulation study. *Journal of Space Science*, **40**(6): 1084−1090. (in Chinese)

[12] Zhang, W., Pan, H. B., Bao, W. Z., et al. 2009. Digital image generation of star map. *Optics and Precision Engineering*, **17**(3): 676−682. (in Chinese)

[13] Han, Y., Sun, H. Y., Li, Y. C., et al. 2010. Simulation of space-based optical measurement serial images. *Optical*

Technique, **36**(1): 93−97. (in Chinese)
[14] Ansys STK Software for Digital Mission Engineering and Systems Analysis. Available from https://www.ansys.com/products/missions/ansys-stk [Accessed 2025−01−14].
[15] Zhang, J., Lou, S. L., Ren, J. C. 2014. A simulation method for space observation image. *Electronics Optics & Control*, **21**(11): 18−23. (in Chinese)
[16] Yan, L. B., Li, J. S., Huang, Z. Y., et al. 2016. Space target optical imaging simulation in space-based system. *Computer Simulation*, **33**(4): 120−124. (in Chinese)
[17] Ouyang, Y., Xu, T. X., Huang, X. B., et al. 2018. An approach to space-debris optical image simulation considering the streak and saturated star-background. *Journal of Physics: Conference Series*, **1060**: 012069.
[18] Wang, Y. P., Niu, Z. D., Wang, D. Y., et al. 2022. Simulation algorithm for space-based optical observation images considering influence of stray light. *Laser & Optoelectronics Progress*, **59**(2): 0229001. (in Chinese)
[19] Liu, P. J., Li, M. Y., Zhang, L. C. 2022. Simulation modeling of infrared images of space targets in jitter state. *Journal of Applied Optics*, **43**(2): 331−338. (in Chinese)
[20] Xu, X. R., Shi, D. L., Xin, M. R., et al. 2020. Imaging simulation of space-based infrared panoramic scanning sensor. In Proceedings of SPIE Second Target Recognition and Artificial Intelligence Summit Forum.
[21] Liu, W. M. 2011. Discussions on the conception of magnitude in Astrophysic. *Journal of Shangqiu Teachers College*, **27**(9): 34−36. (in Chinese)
[22] Myhrvold, N. 2016. Comparing NEO Search Telescopes. *Publications of the Astronomical Society of the Pacific*, **128** (962): 045004.
[23] Yang, X., Zhao, K. X., Gan, Q. B., et al. 2021. Analysis of ground-based and space-based optical observation system warning capabilityof near-Earth asteroids. *Transactions of Beijing Institute of Technology*, **41**(12): 1307−1313. (in Chinese)
[24] Tang, Y. J., Jiang, X. J., Lu, X. M., et al. 2010. Analysis of photometric characteristics of medium and high apogee satellites based on light-reflection model. *Optical Journal*, **30**(3): 763−767. (in Chinese)